BB

CEA/SACLAY
DSM

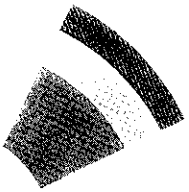

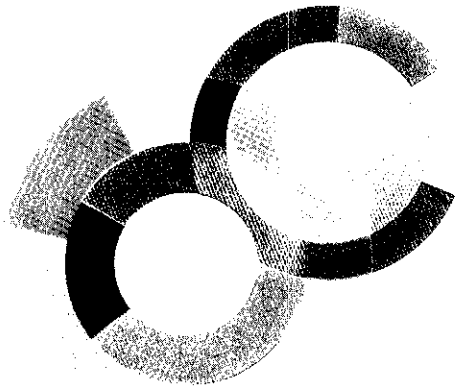

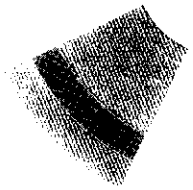

DAPNIA/SPhN-99-35 06/1999

Isotope production in $1 \cdot A\,GeV$ ^{208}Pb on proton reactions

W. Wlazlo, T. Enqvist, P. Armbruster, J. Benlliure, M. Bernas, A. Boudard, S. Czajkowski, F. Farget, R. Legrain, S. Leray, B. Mustapha, M. Pravikoff, K.-H. Schmidt, C. Stéphan, J. Taieb, L. Tassan-got, C. Volant

DAPNIA

3rd International Conference on Accelerator Driven Transmutation Technologies and Applications (ADTTA '99), Praha, Pruhonice, Czech. Republic, June 7-11, 1999

Isotope production in $1 \cdot A\,GeV$ ^{208}Pb on proton reactions

W. Wlazło[a,f], T. Enqvist[b], P. Armbruster[b], J. Benlliure[c], M. Bernas[d], A. Boudard[a], S. Czájkowski[e], F. Farget[d], R. Legrain[a], S. Leray[a], B. Mustapha[d], M. Pravikoff[e], K.-H. Schmidt[b], C. Stéphan[d], J. Taieb[b,d], L. Tassan-got[d], C. Volant[a]

[a] *DAPNIA/SPhN CEA/Saclay, F-91191 Gif-sur-Yvette Cedex, France*
[b] *GSI, Planckstrasse 1, D-64291 Darmstadt, Germany*
[c] *University of Santiago de Compostela, E-15706 Santiago de Compostela, Spain*
[d] *IPN Orsay, BP 1, F-91406 Orsay Cedex, France*
[e] *CEN Bordeaux-Gradignan, F-33175, Gradignan, France*
[f] *Jagiellonian University, Institute of Physics, ul. Reymonta 4, 30-059 Kraków, Poland*

E-mail: ufwlazlo@cyf-kr.edu.pl

Abstract

Spallation reactions of ^{208}Pb at $1 \cdot A\,GeV$ with liquid hydrogen target have been studied using the fragment separator (FRS) facility at the GSI. About 1000 fragmentation residues and fission products from scandium ($Z = 21$) to lead ($Z = 82$) were identified using magnetic rigidities, the energy loss in an ionization chamber and time-of-flight measurements. For each chemical element, the isotopic cross sections of the residual nuclides were obtained. The experiment is described and the experimental cross sections are compared with radiochemical data and with calculations using different intranuclear cascade codes and different evaporation models.

Introduction

Interest in spallation reactions has recently been renewed because of their practical applications in accelerator-driven systems (ADS) [1][2]. In order to understand the spallation process the studies of nuclide production in spallation reactions are very important.

During operation of the ADS a residual radioactivity is accumulated in the irradiated target. Long-lived radioactivity increases the radiotoxicity of the target. Short-lived radioactivity can induce some problems of maintenance of the hybrid system. The gaseous and corrosive isotopes produced inside the target can damage the target and its container. To predict these effects it is necessary to improve the experimental knowledge of the spallation residues production cross sections.

Several numerical simulation codes are available to design the accelerator driven systems. However, the predictions of residue production do not fully reproduce the existing data [3]. Actually, residue production cross sections are of the highest importance in order to improve and benchmark used codes. A direct measurement performed before most of the radioactive decays is in that sense an improvement to the existing radiochemical analysis of activated targets.

The present contribution reports on an inverse-kinematics experiment in which a ^{208}Pb beam was impinging on a liquid hydrogen target at $1 \cdot A\ GeV$. In this experiment performed at the fragment separator at GSI, a complete survey of isotopic production cross sections of all elements from scandium (Z=21) to lead (Z=82) formed in this spallation

reaction was obtained with a high accuracy down to 0.1 *mbarn*. In addition, the recoil velocity distributions of all these reaction products were determined.

The present experimental results are compared with radiochemical data and with results of Monte-Carlo calculations. The differences between them are discussed.

Experimental procedure

The experiment was performed at the fragment separator (FRS) [4],(see fig. 1) at GSI in Germany. The FRS is a two-stage magnetic spectrometer with dispersive intermediate image plane and achromatic final focal plane. The primary beam of ^{208}Pb, accelerated in the heavy-ion synchrotron SIS to an energy of $1 \cdot A\ GeV$, impinged on the liquid hydrogen target mounted at the entrance of the FRS. The projectile-like fragments produced in the target were separated from the beam in the first part of the FRS. In the dispersive central focal plane their magnetic rigidities were determined by a plastic scintillator detector. This detector measures the horizontal position of each ion and gives a start signal of the time-of-flight between central and final focal plane (36.13 m). In case of isotopes with the highest nuclear charges ($64 < Z < 83$) an achromatic degrader [6] (5.3 g/cm^2 or 5.9 g/cm^2 of Al) was placed at the central dispersive focal plane in order to obtain a better Z resolution. In the second half of the fragment separator the ions were deflected again and refocused at the final focal plane. Their magnetic rigidities were determined from their position at the central and final focal planes.

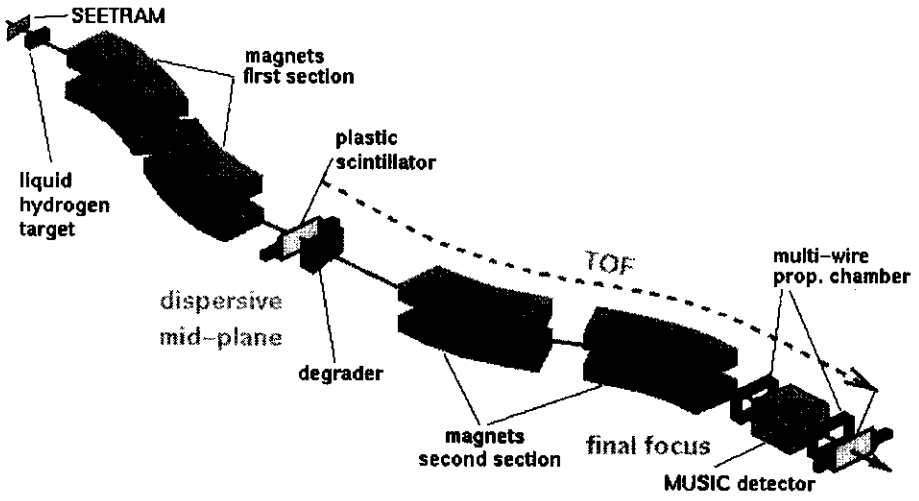

Figure 1: Experimental setup for the isotope production cross section measurement with the FRS operated in achromatic mode.

At the final focal plane the following detectors were placed: *(i)* a plastic scintillator detector to measure the position and to give the stop signal for the time-of-flight, *(ii)* a MUSIC (MUltiple-Sampling Ionization Chamber) [7] detector to measure the energy loss and also the position of the ions. In addition, to tune the separator, several position-sensitive multiwire proportional counters were used at the central and final focal plane.

To separate all residues with nuclear charges from 21 to 82 it was necessary to use two independent methods for the analysis. In case of isotopes with high nuclear charges ($64 < Z < 83$) the resolution of the MUSIC detector was not sufficient to separate clearly all Z. The nuclear charge of these fragments was deduced from their energy loss in the

thick degrader placed at the central focal plane. The method for calculating that energy loss induced by the thick degrader from the difference of magnetic rigidities in the first and the second part of the FRS, and from the time-of-flight in the second part of the FRS is given in ref. [8].

The A/Z ratios of the isotopes produced were determined by their magnetic rigidities and the time-of-flight in the second part of the fragment separator.

Ions passing through the fragment separator are not always fully stripped and this can cause problems for their identification. By comparing the energy-loss caused by the degrader with the energy-loss signal of the MUSIC detector, the analysis can be restricted to those ions which are fully stripped in both sections of the fragment separator. The contribution of incompletely stripped ions is less than 5% for residues with nuclear charges below Z=70. In case of residues close to the projectile it can reach a level of 16%. These corrections were obtained from data collected in the present experiment and applied to the production cross sections.

The nuclear charges of light ions ($20 < Z < 66$) were deduced from the energy loss in the MUSIC detector. The absolute charge calibration for these fragments was obtained by following continuously the charge spectra with overlaps in various settings of the magnetics fields in the spectrometer, starting from the charge of the beam ($Z = 82$). The probability for misidentification in charge number due to the Z resolution is below 3%.

The measured counting rates, attributed to a specific isotope, were normalized to the number of projectiles as recorded with the Secondary Electron Emission TRAnsmission beam Monitor (SEETRAM) (8.9 mg/cm^2 aluminum) [5] and corrected for the dead time of the acquisition system.

The target of 87.3 mg/cm^2 of liquid hydrogen is contained inside titanium windows of 36 mg/cm^2 total thickness. Therefore, the reaction rates in the titanium windows were measured separately and subtracted from the reaction rates in the full target.

The rate of the secondary reactions of the residues in the degrader and all detectors was estimated using a total cross section formula [9]. In case of the measurements with degrader this rate varies between 20 and 50% for Sc and Pb residues, respectively. The correction for secondary reaction inside the hydrogen target was estimated from reaction rates obtained in the present experiment.

Since the momentum acceptance of the fragment separator amounts to 3%, 75 different values of the magnetic field were set in steps of 2% in order to cover entire (Z,N) production and to reconstruct complete velocity distribution for each fragment.

The transmission losses in the fragment separator can be attributed to its limited longitudinal momentum acceptance and to its limited angular acceptance. The limitation in longitudinal momentum is overcome by constructing full velocity distributions from the data of many different magnetic settings. The angular transmission of the FRS was calculated using the method described in ref. [10] taking into consideration the kinematical properties of the fragments determined by the production mechanism.

Due to the precision of all used corrections a systematic error should be applied to the cross sections for production of spallation residues and fission fragments, ranging from 10% to 30%, respectively.

Results

For each identified isotope, its velocity in the center of the target was determined using the magnetic rigidity in the first part of the FRS. The velocities were transformed into the projectile rest-frame. A correction due to energy loss of the projectile and the fragment was applied assuming that the nuclear reaction takes place at half thickness of the target.

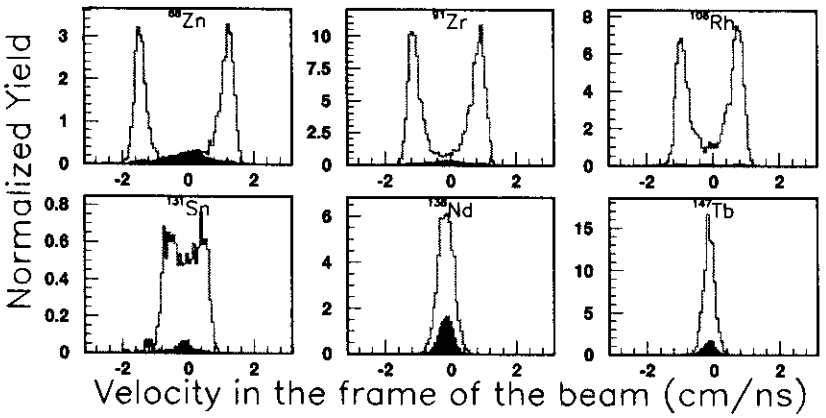

Figure 2: Velocity distributions of selected isotopes: ^{68}Zn ($Z = 30$), ^{91}Zr ($Z = 40$), ^{106}Rh ($Z = 45$), ^{131}Sn ($Z = 50$), ^{136}Nd ($Z = 60$), ^{147}Tb ($Z = 65$). Open histogram - yields obtained in the full target. Filled histogram - yields obtained in the titanium windows.

Fig. 2 shows the velocity distributions of several isotopes. The isotopes closer to the beam ($Z > 60$) have velocity distribution with one peak, of which the mean value is a little below the beam velocity. Such shape of velocity distribution can be attributed to the fragmentation mechanism. Lighter isotopes ($Z = 21$ to 50) shows double-humped velocity distributions which is attributed to fission. Due to the limited angular acceptance of the FRS, only those fission products which are emitted in forward or backward direction can be registered. The position of the peaks is determined by the Coulomb repulsion of fission fragments. In the intermediate case of Z between 50 and 60, signatures of both fission and fragmentation processes are visible.

From the velocity distributions, information about the momentum transfer induced in the spallation reactions can be obtained. That information is valuable for evaluating the material damage which is necessary to design the window and the container of the spallation target in an ADS system.

In figure 3 the isotopic production cross sections measured in the present work are summarized on the chart of nuclides. According to the velocity distributions of the fragments (see fig. 2), the charge region between $Z = 21$ and $Z = 55$ is due to fission process. These isotopes are located in the stability valley. The residues with charges above $Z = 55$ are mainly produced by the spallation-evaporation process. They populate a corridor, half way between the valley of stability and the proton drip line.

The comparison with data obtained by radiochemical methods in the direct-kinematics experiment[12] is shown in fig. 4. In this picture the ratio between our data and radiochemical data is plotted for the independent and cumulative yields. In case of independent yields (isotopes shielded by long-lived precursor in the decay chain) the agreement is satisfactory except for ^{93}Mo and ^{131}Ba. The radiochemical cumulative yields produced partially by radioactive decay of their mother-nucleus show variation within a factor of 2 compared to our (inverse kinematics) data where all isotopes are measured before any

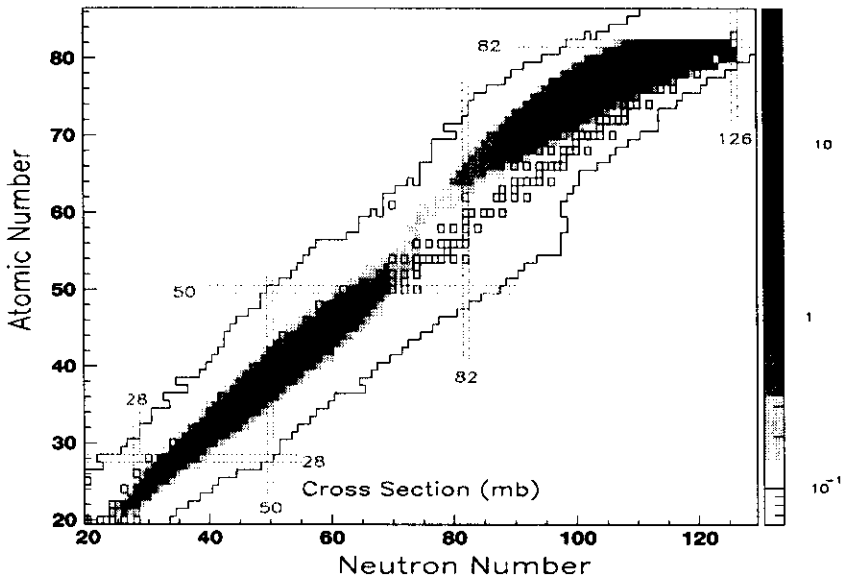

Figure 3: Measured isotopic cross sections for the reaction of $1 \cdot A\,GeV$ $^{208}Pb + p$ on the chart of nuclides. Stable isotopes are marked by open squares.

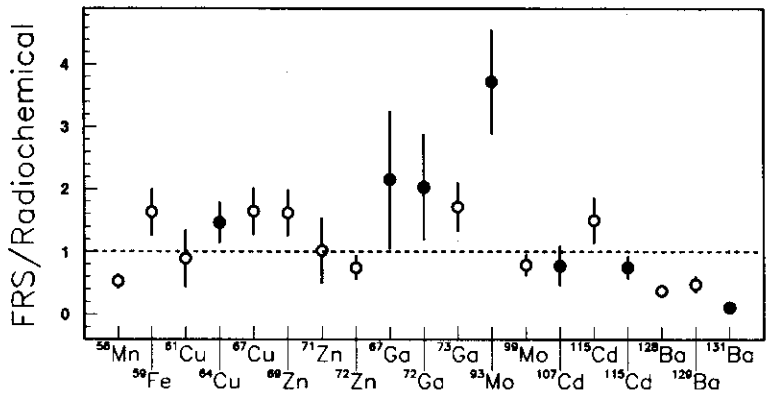

Figure 4: Ratio between our and radiochemical data. o - cumulative yields. • - independent yields (shielded isotopes).

radioactive decay.

The understanding of the spallation process, can be tested by a comparison between the data and a two-step model. In the first step, the nucleon-nucleon interactions inside the nucleus lead to the loss of some nucleons, and an excited prefragment is created. This process can be described by the intranuclear cascade model. In the second step, the prefragment can fission or deexcites by emission of nucleons, light particles or gammas. The evaporation models describe this stage of the reaction.

In order to study the influence of the first step, calculations using two different intranuclear cascade models combined with the same evaporation code were performed. Figure 5 shows comparisons of the data obtained in our experiment with predictions given by Bertini [14] and ISABEL [15] intranuclear cascade codes followed by the Dresner [16] evaporation code. These two code configurations are part of the commonly used LAHET Code System from Los Alamos [17]. In the upper part of figure 5, all shapes of the isotopic distributions from both numerical calculations have some distortions in comparison with the experimental data. The isotopic distributions of heavier Z are shifted with respect

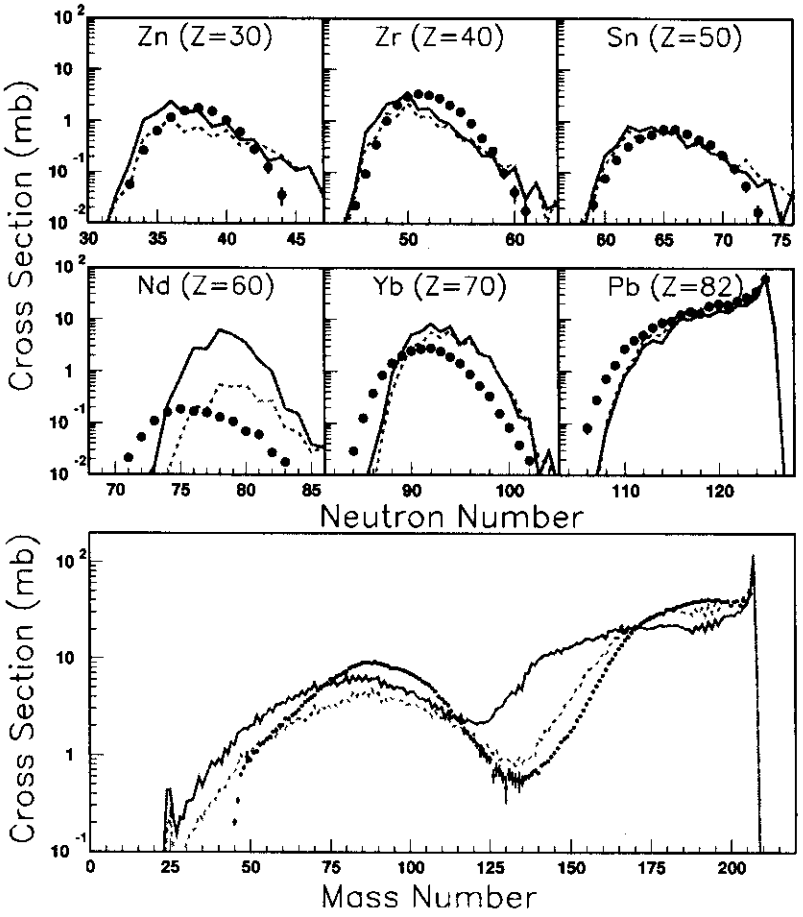

Figure 5: Comparison of data obtained in our experiment (points) with predictions given by two different intranuclear cascade codes of Bertini (solid line) and ISABEL (dashed line) followed by the same evaporation code of Dresner. Upper part: Isotopic distributions of Zn, Zr, Sn, Nd, Yb and Pb. Bottom part: Mass distributions.

to the experimental ones towards the neutron-rich side. This can be due to the fact that the prediction of the neutron-proton evaporation ratio in the Dresner code is not satisfying. Moreover, isotopic distributions obtained by these two numerical calculations have different magnitudes. Especially, when we look at isotopic distributions of elements close to Nd. This effect is better visible on the mass distribution (the bottom part of figure 5), where we can observe an overproduction of isotopes near the mass $A = 140$ and underproduction of isotopes close to the mass $A = 208$, in case of the Bertini code. This can be explained by too high excitation energies of the prefragments after the intranuclear-cascade step, which results in evaporation more particles and finally in producing lighter nuclides. In results obtained by the ISABEL model followed by the Dresner code, this effect is less visible, probably due to the lower excitation energy of prefragments after the intranuclear step. Figure 5 also shows that both models included in the LAHET Code System underpredict the fission contribution and give the mass distributions shifted to lower masses than measured.

Importance of the evaporation-fission step was examined by performing calculations using the intranuclear cascade code of Cugnon [18] followed by two different evaporation codes: from Dresner [16] and a code elaborated in GSI [19]. In the upper part of figure 6 the comparison of isotopic distributions is shown. In case of the Cugnon-GSI model we

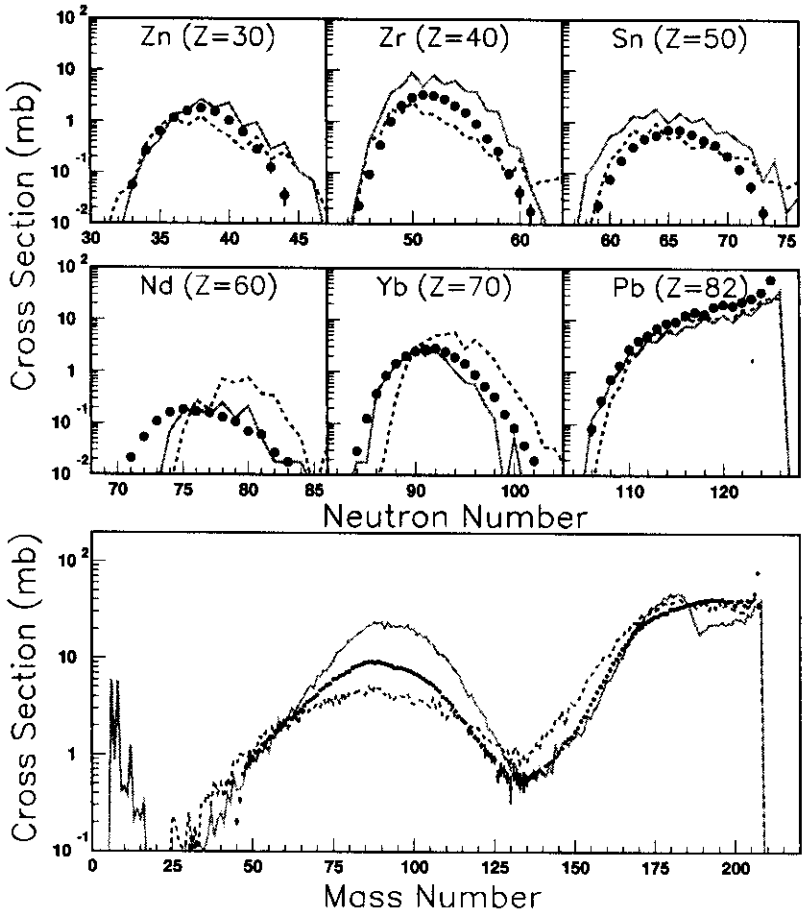

Figure 6: Comparison of data obtained in present experiment (points) with predictions given by two different evaporation codes: from Dresner (dashed line) and the GSI code (solid line) preceded by the same intranuclear cascade code of Cugnon. Upper part: Isotopic distributions of Zn, Zr, Sn, Nd, Yb and Pb. Bottom part: Mass distributions.

found that the best results are obtained when the prefragments after the intranuclear-cascade step have higher excitation energy. This effect can be achieved by earlier stopping the cascade. The duration time of the cascade stage in the used Cugnon-GSI model was adjusted to be 25% shorter than the standard one [18]. Isotopic distributions of heavier elements obtained by the intranuclear cascade code of Cugnon followed by the evaporation code of Dresner are shifted with respect to the experimental ones to the neutron-rich side, what can be explained by incorrect prediction of the neutron-proton evaporation competition in the model of Dresner (see also fig. 5). The shapes of the isotopic distributions are better reproduced by the intranuclear cascade model of Cugnon followed by the GSI evaporation code. In the bottom part of figure 6 mass distributions obtained by the Cugnon code followed by two different evaporation codes are compared with the experimental data. In case of the Cugnon code followed by the Dresner code we can observe a similar behavior as that presented by the ISABEL code followed by the same evaporation code of Dresner, indicating problems with a slightly too high excitation energy of the prefragment. In contrary, the GSI evaporation code works much better with the code of Cugnon. Notice that with this combination a higher excitation energy is required after the cascade stage in contrast with what is observed with the Cugnon-Dresner model. The Cugnon-GSI model gives the best results according to the shape

of the isotopic distributions. However, the fragmentation part of the mass distribution curve exhibits some distortions and the fission contribution is overpredicted by this code configuration. The magnitude of the calculated fission cross section is extremely sensitive to the suppression of fission at high excitation energies due to dissipation. Therefore the data are an interesting source of information on the magnitude of nuclear viscosity [20].

Summary

- The fragment-separator facility at GSI has been used to determine the production cross sections and momentum distributions of about 1000 isotopes from spallation reactions of $1 \cdot A\ GeV\ Pb$ with protons. These data can be used directly to calculate the residual radioactivity and the amount of corrosive isotopes that are produced inside the spallation target during the operation of the accelerator-driven system.

- The reaction mechanisms responsible for the creation of the spallation residues have been studied using the full isotopic distributions and the kinematical properties of the fragments. The recoil momentum transfers can be valuable for the radiation material damage evaluations.

- The detailed comparison of the obtained cross sections with radiochemical data shows an over all satisfactory agreement.

- The numerical calculations using four different combinations of three intranuclear cascade codes and two evaporation codes have been performed. The results of those calculations show that at present no model can guarantee a prediction of the residual nuclei production within a factor 2 to 3. In order to refine and benchmark existing Monte Carlo codes, our group has already measured the residue production cross section in the following reactions: $1 \cdot A\ GeV\ ^{238}U + p$, $0.8 \cdot A\ GeV\ ^{197}Au + p$ and $0.5 \cdot A\ GeV\ ^{208}Pb + p$.

This research was partially supported by the Polonium Program 1999, Dossier N° 99066.

References

[1] C. D. Bowman et al., Nucl. Instrum. Methods A 320 (1992) 336.
[2] C. Rubbia et al, CERN report AT 93-47 (ET).
[3] R. Michel, P. Nagel, *International Codes and Model Intercomparison for Intermediate Energy Activation Yields* OECD, (1997).
[4] H. Geissel et al. Nucl. Instrum. Methods, B70 (1992) 286.
[5] E. Hanelt et al., GSI Scientific Report 1990, 291 (1991).
[6] K.-H. Schmidt et al., Nucl. Instr. Methods. A260 (1987) 287.
[7] K.-H. Schmidt et al., Nucl. Phys. A452 (1992) 699.
[8] L. Tassan-got et al., in preparation.
[9] C. J. Benesh et al., Phys. Rev. C, Vol. 40, (1989) 1198.
[10] J. Pereira et al., *Studies of the angular transmission at the GSI projectile fragment separator (FRS)*, GSI (1998).

[11] B. C. Barashenkov, *Cross Sections of Interactions of Particle and Nuclei with Nuclei*, JINR, Dubna, (1993).
[12] R. Wolfgang et al., Phys. Rev. vol. 103, no. 2 (1956).
[13] E. J. Moniz et al., Phys. Rev. Lett. 26 (1971) 445.
[14] H.W. Bertini, Phys. Rev. 188 (1969) 1711.
[15] Y. Yariv, Z. Fraenkel, Phys. Rev. C20 N 6 (1979) 2227.
[16] L. Dresner, *EVAP - A Fortran Program for Calculating the Evaporation of Various Particles from Excited Compound Nuclei*, ORNL-TM-196, Oak Ridge National Laboratory (April 1962).
[17] R. E. Prael and H. Lichtenstein, Los Alamos-UR-89-3014 (1989).
[18] J. Cugnon et al., Nucl. Phys. A 620 (1997) 475.
[19] J. Benlliure et al., Nucl. Phys. A 628 (1998) 458.
[20] J. Benlliure et al.,*Fourth International Conference on Dynamical Aspects of Nuclear Fission*, Casta-Papiernicka, Slovak Republic, October 1998.